

## Article

# Obtaining and Characterizing New Types of Materials Based on Low-Density Polyethylene and Thermoplastic Starch

Maria Daniela Stelescu<sup>1</sup>, Ovidiu-Cristian Oprea<sup>2,3,\*</sup> , Ludmila Motelica<sup>2</sup> , Anton Ficai<sup>2,3</sup> ,  
Roxana-Doina Trusca<sup>2</sup>, Maria Sonmez<sup>1</sup>, Mihaela Nituica<sup>1</sup> and Mihai Georgescu<sup>1</sup>

<sup>1</sup> Division Leather and Footwear Research Institute, National Research & Development Institute for Textiles and Leather, 93 Ion Minulescu St., 031215 Bucharest, Romania; dmstelescu@yahoo.com (M.D.S.); maria.sonmez@icpi.ro (M.S.); mihaelavilsan@yahoo.com (M.N.); mihai.georgescu@icpi.ro (M.G.)

<sup>2</sup> Faculty of Chemical Engineering and Biotechnologies, National University of Science and Technology POLITEHNICA Bucharest, 1-7 Polizu St., 011061 Bucharest, Romania; ludmila.motelica@upb.ro (L.M.); anton.ficai@upb.ro (A.F.)

<sup>3</sup> Academy of Romanian Scientists, 3 Ilfov St., 050044 Bucharest, Romania

\* Correspondence: ovidiu.oprea@upb.ro

**Abstract:** Significant interest is devoted to the development of new polymer blends by using concepts of the circular economy. Such materials have predetermined properties, are easy to recycle, ecological, and have a low carbon footprint. This research presents obtaining and characterization of polymer blends based on low-density polyethylene (LDPE) and thermoplastic starch (TPS). In the first stage, TPS was obtained through the gelatinization process, and, in the second stage, mixtures of LDPE and TPS were obtained through a melt mixing process at 150 °C for 7 min. The physical–mechanical characteristics of the samples, like hardness, elongation at break, rebound resilience, and tensile strength, were determined. The sample containing maleic anhydride grafted low-density polyethylene (LDPE-g-MA) as a compatibilizer shows improvements in elongation at break and tensile strength (by 6.59% and 40.47%, respectively) compared to the test sample. The FTIR microscopy maps show that samples containing LDPE-g-MA are more homogeneous. The SEM micrographs indicate that TPS-s is homogeneously dispersed as droplets in the LDPE matrix. From the thermal analysis, it was observed that both the degree of crystallinity and the mass loss at high temperature are influenced by the composition of the samples. The melt flow index has adequate values, indicating good processability of the samples by specific methods (such as extrusion or injection).

**Keywords:** low-density polyethylene (LDPE); thermoplastic starch (TPS); sustainable; polymer blends; thermal properties; SEM



**Citation:** Stelescu, M.D.; Oprea, O.-C.; Motelica, L.; Ficai, A.; Trusca, R.-D.; Sonmez, M.; Nituica, M.; Georgescu, M. Obtaining and Characterizing New Types of Materials Based on Low-Density Polyethylene and Thermoplastic Starch. *J. Compos. Sci.* **2024**, *8*, 134. <https://doi.org/10.3390/jcs8040134>

Academic Editor: Francesco Tornabene

Received: 8 March 2024

Revised: 2 April 2024

Accepted: 3 April 2024

Published: 5 April 2024



**Copyright:** © 2024 by the authors. Licensee MDPI, Basel, Switzerland. This article is an open access article distributed under the terms and conditions of the Creative Commons Attribution (CC BY) license (<https://creativecommons.org/licenses/by/4.0/>).

## 1. Introduction

Oil-based plastic materials have experienced significant development in recent decades, both due to their low cost and specific properties, which have enabled their use in many domains [1]. Since waste from discarded plastic products is non-biodegradable and significantly affects the environment, several regulations have been applied worldwide regarding their reduction as well as the development of new sustainable and environmentally friendly materials [2]. For these reasons, new materials with a reduced impact on the environment have been developed. Among them, thermoplastic starch (TPS) is particularly important [3]. TPS, as opposed to dry starch, is capable of flow, and, hence, when mixed with other synthetic polymers, it can behave in a manner similar to conventional polymer blends [4]. Nevertheless, TPS has multiple advantages: it is completely biodegradable, is non-toxic, has a low cost, is obtained from renewable sources, and does not affect the environment [5–7]. TPS cannot be used as such for various industrial applications due to its inadequate mechanical and chemical properties (like fragility or water sensitivity) [8] or low thermal stability [9]. The hydrophilic nature of TPS [10] and moisture-induced

recrystallization (retrogradation) usually lead to an increase in rigidity and separation of the polymer/solvent phases [11,12]. In order to remedy these disadvantages, TPS can be mixed with hydrophobic polymers [13]. Several factors influence the mechanical properties of these blends: starch characteristics like granule morphology, the amylose to amylopectin ratio, the type and quantity of compatibilizers, use of inorganic fillers, using recycled polymers, the type of plasticizers, and the processing technique [14].

Several studies have shown that, by mixing TPS with other non-biodegradable synthetic polymers, new materials can be obtained with low cost, good mechanical properties, and improved biodegradability in various environmental conditions [15,16]. Thus, several researchers have obtained and characterized mixtures based on TPS with polycaprolactone [17], polybutyrate adipate terephthalate [18,19], polylactide [20,21], polyethylene [22,23], polypropylene [24], etc. Of these, most studies have been performed on plasticized starch and low-density polyethylene (LDPE) mixtures, which can be used in packaging [25] and in other industrial applications [26]. As TPS is polar and LDPE is non-polar, their blends are immiscible due to high interfacial tension. These immiscible blends are characterized by distinct phase morphologies, coalescence of the dispersed phase, and poor mechanical properties. In order to obtain mixtures with suitable properties for different applications, small amounts of compatibilizer can be added. The compatibilizer will reduce the interfacial tension and improve the adhesion between the two phases, forming and stabilizing the desired morphology, thus leading to improvement in the mechanical properties [27,28]. The literature indicates the use of several types of compatibilizers for TPS/LDPE blends, such as ethylene-co-acrylic acid copolymer [29], ethylene-vinyl alcohol [30], and polyethylene-grafted maleic anhydride (PE-g-MA) [31,32]. Of these, PE-g-MA is the most frequently used because it leads to improved compatibility between LDPE and TPS. This improvement could be attributed to esterification reactions between the maleic anhydride groups of PE-g-MA and the hydroxyl groups of starch [31,32].

Literature reports indicate inhomogeneous blends obtained from LDPE and TPS [33,34], with continuous domains made of TPS, highly prone to biodegradation. In other cases, when LDPE-g-MA compatibilizer is used, poor homogeneity is assessed from DSC peaks, while SEM study occurs without TPS etching, therefore being inconclusive [35]. Even the use of starch nanocrystals does not yield a homogenous dispersion [36]. In most of these studies, the starch was plasticized with glycerol or with a glycerol/water mixture. In our study, we present obtaining and characterization of highly homogenous mixtures based on LDPE and TPS. We used TPS obtained from starch plasticized with glycerol and sorbitol, which has an addition of citric acid in order to improve its mechanical properties. This type of TPS will improve the properties of subsequent mixtures with other polymers. We have obtained polymer blends with just under 10% TPS-s and analysed the effect of adding a small amount of ethylene-propylene-terpolymer rubber and LDPE-g-MA compatibilizer on the structural, morphological, mechanical, and thermal properties of the resulting mixtures.

## 2. Experimental

### 2.1. Materials

The following materials were used to obtain the mixtures: (1) low-density polyethylene (LDPE) TIPOLEN MF 243-51 from MOL Petrochemicals Co., Ltd., Hungary; (2) thermoplastic starch (TPS-s) made using soluble starch obtained from potatoes from Lach-Ner, Czech Rep. as polymer matrix, two types of plasticizers, namely glycerol from Lach-Ner and sorbitol from Thermo Scientific, Czech Rep., and citric acid anhydrous from Reanal Laborvegyszer Kft., Budapest, Hungary; (3) ethylene-propylene-terpolymer rubber (EPDM) Nordel 47130 from Dupont Elastomer; (4) polyethylene grafted with maleic anhydride (LDPE-g-MA) Admer NF 468E from Mitsui Chemicals Europe GmbH, Germany. The main characteristics of the materials used are presented in Table 1.

**Table 1.** Main characteristics of materials used.

Material	Producer	Role	Characteristics
Low-density polyethylene (LDPE) TIPOLEN MF 243-51	MOL Petrochemicals Co., Ltd., Tiszaújváros, Hungary	Polymer matrix	MFR—Melt Mass Flow Rate (190 °C, 2.16 kg) 20 g/10 min; density: 0.922 g/cm <sup>3</sup> ; Vicat softening temperature 90 °C
Soluble starch from potatoes	Lach-Ner, Neratovice Czech Republic	Organic filler	Water insoluble substances 0.28%, loss on drying (105 °C) 17.52%
Glycerol	Lach-Ner, Neratovice, Czech Republic	Plasticizer	Acidity 0.02%, density 1.26 g/cm <sup>3</sup>
Sorbitol	Thermo Scientific, Brno, Czech Republic	Plasticizer	D-sorbitol 97%
Citric acid anhydrous	Reanal Laborvegyszer Kft., Budapest, Hungary	Compatibilizing agent	C <sub>8</sub> H <sub>8</sub> O <sub>7</sub> , molecular weight of 192.13 g/mol, purity 99.8%, sulphate ash < 0.02%, chlorides (Cl) < 0.0005%, sulphates (SO <sub>4</sub> ) < 0.02%, oxalates (C <sub>2</sub> O <sub>4</sub> ) < 0.05%
LDPE-g-AM Admer NF 468E	Mitsui Chemicals Europe GmbH, Düsseldorf, Germany	Compatibilizing agent	Density 0.92 g/cm <sup>3</sup> , melting point 120 °C
EPDM Rubber Nordel 47130	Dupont Elastomer, Wilmington, DE, USA	Elastomer	Containing 67% (wt) ethylene and 4.9% (wt) 5-ethylidene-2-norbornene; Degree of crystallinity 9%, density 0.97 g/cm <sup>3</sup> ; carbon black amount: 28% M <sub>w</sub> = 308,000; T <sub>c</sub> = 8 °C

### 2.2. Obtaining Thermoplastic Starch (TPS)

In order to obtain thermoplastic starch, ingredients were weighed and mixed in a Berzelius beaker in the following mass ratio starch:glycerol:sorbitol:citric acid of 60:20:20:2. After homogenization, ingredients were introduced in an internal Plasti-Corder Brabender mixer, where the gelatinization of the starch took place. The resulting thermoplastic starch—TPS-s—was obtained at 120–140 °C using a mixing rate of 30–80 rpm for 10 min.

### 2.3. Obtaining Mixtures and Test Samples

The composition of the obtained blends is presented in Table 2. The polymeric mixtures were obtained using a Plasti-Corder Brabender internal mixer 350E (Duisburg, Germany), and the obtained experimental data were processed using the Brabender Mixer WinMix software, version 3.2.30.

**Table 2.** Composition of mixtures.

Ingredients	Sample Code			
	A0	A1	A2	A3
LDPE, (g)	260	235	225	200
TPS-s, (g)	-	25	25	25
LDPE-g-AM, (g)	-	-	10	10
EPDM, (g)	-	-	-	25

The mixer chamber was calibrated for each sample. Pre-weighted quantities of ingredients were inserted in the mixer chamber and the program was started. The rotor speed was 30 rpm in the first 3 min and increased to 80 rpm for the next 5 min. Figure 1 shows the variation in torque regarding time when obtaining the mixtures.

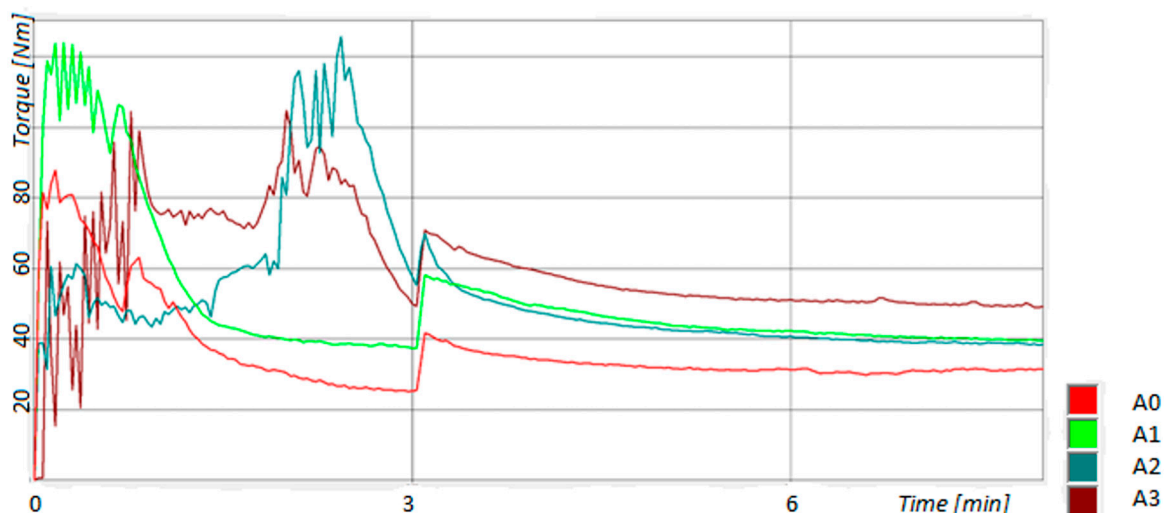


**Figure 1.** Diagram showing the variation in torque versus time when obtaining the blends on Plasti-Corder Brabender.

It can be seen from the Figure 1 that the mixtures presented the highest torque values in the first 3 min of mixing. There is another increase in torque when the rotational speed is increased from 30 rpm to 80 rpm, after which the torque decreases to an equilibrium value, indicating the proper homogenization of the ingredients. Torque is influenced by the viscosity in melt state at the working temperatures of mixtures [37,38]. Thus, the blends containing TPS-s show higher torque values at equilibrium (at the end) than the sample containing only LDPE—sample A0 [39]. When replacing an amount of LDPE with EPDM elastomer (which is more amorphous than LDPE), an increase of 28.75% in equilibrium torque can be observed [37]. The influence of adding LDPE-g-MA on torque variation in time is similar to that reported by Abdul Majid et al. [40]. As the reported samples have a low TPS-s content, under 10%, the equilibrium torque value change is small. Table 3 shows some parameters recorded during the process of obtaining the mixtures. The mechanical energy input required to obtain the mixtures increases as the torque increases. The temperature during obtaining the mixtures decreases initially as a result of the introduction of the ingredients at room temperature in the mixer, after which it increases due to the temperature in the mixing chamber (150 °C) as well as due to the increase in the shear moment, the effect being reported previously [41].

**Table 3.** The characteristics obtained using the Plasti-Corder Brabender during the preparation of the mixtures.

Sample Code	Specific Energy, [kJNm/g]	Torque Variation Range, [Nm]	Temperature Variation Range, [°C]
A0	0.4	31.7–87.9	105–153
A1	0.7	37.6–124	103–155
A2	0.7	36.9–113.3	92–154
A3	0.8	47.5–104.5	80–159

The resulting mixtures were used to make plates by compression moulding, using specific moulds and the laboratory electrical press (Fortune Presses model no. TP 600 manufactured by Fontijne Grotnes, Vlaardingen, The Netherlands). The processing parameters were preheating for 2 min at the temperature of 170 °C, modelling at the temperature of 170 °C, 5 MPa, and time 6 min, followed by the cooling stage down to 45 °C for 10 min and 5 MPa. Plates with dimensions 150 × 150 × 2 mm<sup>3</sup> and 50 × 50 × 6 mm<sup>3</sup> were obtained from which test specimens were punched.

## 2.4. Specimen Characterization

*Static tensile tests* were carried out using type 1 dumb-bell-shaped specimens ( $6 \pm 0.4$  mm width at narrow portion and  $2 \pm 0.2$  mm thickness) according to [42], with the testing speed of 50 mm/min at room temperature; five test specimens were used for each sample, and the median values for each property were selected. *Tearing strength* test was carried out using angular test pieces with thickness of  $2.0 \pm 0.2$  mm according to [43]; the test speed was 500 mm/min, five test specimens were used for each sample, and the arithmetic mean of the obtained values was found. *Hardness* was measured in °Sh D (scale specific for hard materials) by using 6 mm thick samples according to [44]. A minimum of five hardness measurements were taken at different positions on the test specimen and the average value was determined. *Rebound resilience* was determined according to [45] using the Schob pendulum; 2 test pieces with a thickness of  $6.3 \pm 0.3$  mm were used, 3–7 impacts with the same speed were applied to each test piece, and the average of the median values of the two test pieces was calculated. *Melt flow index (MFI)* of the samples was measured by means of an extrusion through a 2 mm die (capillary rheometer—Melt Flow Index—Haake) at 200 °C, preheating for 4 min, and 2.16 kg force was used according to [46].

*Fourier Transform Infrared Spectroscopy (FTIR) spectra* of samples were obtained using Nicolet iS50 FT-IR spectrophotometer regarding wave numbers ranging from  $400\text{ cm}^{-1}$  to  $4000\text{ cm}^{-1}$  using attenuated total reflection (ATR). The FTIR 2D maps were recorded with a Nicolet iN10 MX (Nicolet, Waltham, MA, USA) in the domain  $4000\text{--}650\text{ cm}^{-1}$ .

Scanning electron micrographs for determination of the films' homogeneity and surface morphology were obtained with a QUANTA INSPECT F50, FEI Company, Eindhoven, The Netherlands. For visualization of TPS dispersion in LDPE matrix, cryo-fractured samples (at liquid nitrogen temperature) were immersed for 48 h in HCl 6N at 60 °C, as indicated in [33,34]. Samples were coated with gold to ensure conductivity.

Thermal behaviour was followed with a STA 449C F3 system, TG-DSC (thermogravimetry—differential scanning calorimetry) from Netzsch (NETZSCH-Gerätebau GmbH, Selb, Germany) between 20 and 900 °C in dynamic (50 mL/min) air atmosphere. The evolved gases were transferred through heated transfer lines and analysed on the fly with the help of an FTIR Tensor 27 from Bruker (Bruker Co., Ettlingen, Germany) equipped with an internal thermostatic gas cell.

## 3. Results and Discussion

### 3.1. Physical–Mechanical Properties

Some of the most important physical–mechanical characteristics of the samples are presented in Table 4. The analysed mixtures have a rebound resilience (*elasticity*) of 16–18%, and a decrease of 11.11% is noticed in samples containing TPS-s, indicating that plasticized starch can reduce the elasticity of LDPE.

**Table 4.** Physical–mechanical characteristics of the samples.

Characteristics	Sample Code				
	TPS-s	A0	A1	A2	A3
Rebound resilience, %	-	$18.0 \pm 0.33$	$16.0 \pm 0.58$	$16.0 \pm 0.58$	$16.0 \pm 0.58$
Tensile strength, N/mm <sup>2</sup>	$4.25 \pm 0.04$	$15.4 \pm 0.67$	$13.36 \pm 0.16$	$14.24 \pm 0.17$	$11.29 \pm 0.05$
Elongation at break, %	$40 \pm 4.41$	$100.0 \pm 2.89$	$60.0 \pm 2.89$	$80.0 \pm 2.89$	$40.0 \pm 0.58$
Tearing strength, N/mm	$20.5 \pm 0.26$	$99.9 \pm 4.45$	$55.6 \pm 4.73$	$78.1 \pm 1.67$	$61.0 \pm 4.69$
Hardness, °Sh D	$31 \pm 0.58$	$59 \pm 0.33$	$56 \pm 0.33$	$55 \pm 0.33$	$53 \pm 0.58$
MFI at 200 °C and 2.16 kg, g/10 min	-	$29.8 \pm 0.17$	$26.1 \pm 0.17$	$22.9 \pm 0.97$	$14.9 \pm 0.21$

The values of *tensile strength* and *tear strength* decrease by 13.25% and 44.34%, respectively, by mixing LDPE with TPS-s (sample A1 compared to sample A0); an improvement

in these characteristics is noticed (6.59% and 40.47%, respectively) in sample A2, which contains LDPE-g-AM compatibilizing agent, compared to A1. When adding EPDM elastomer (sample A3), decreases of 20.72% and 21.9%, respectively, can be observed for tensile strength and tear strength, which may be due to a reduction in the crystalline phase percentage as a result of adding the elastomer. Therefore, the values of tensile and tear strength of polymer blends depend on the individual values of each component but also on the compatibility between mixture components [47].

*Elongation at break* has low values, of 40–100% for all samples, and shows a decrease when adding TPS-s in LDPE, which may indicate that starch macromolecules with lower molecular weight than polyethylene existing in the samples have a lower resistance to the action of strong forces. In the A2 mixture containing LDPE-g-AM, a 33.33% improvement in elongation at break can be observed, which can be due to the improvement in the adhesion between the two phases (the polar one—TPS-s and the non-polar one—LDPE) as a result of esterification reactions between LDPE-g-MA and TPS-s [31,32]. For the A3 mixture, a reduction in this characteristic (by 50%) can be observed, which could be due to the reinforcing effect of carbon black, which is the active filler from EPDM (28% mass ratio) [48,49].

*The hardness* of samples (Table 4) in the normal state is 53–59 °Sh D. When adding TPS-s, LDPE-g-AM and EPDM in the LDPE matrix, a slight decrease in hardness value can be observed compared to the control sample (LDPE), which may be due to a reduction in the crystalline phase percentage by adding low-molecular-weight compounds, grafted polymers, and elastomers, respectively, with a high percentage of amorphous phase. The behaviour of the samples after *accelerated ageing for 168 h at 70 °C* is very good, with the variation in hardness being only  $\pm 3$  °Sh D.

*The melt flow index (MFI)* values at 200 °C and a pressing force of 2.16 kg (Table 4) for the analysed samples vary between 14.9 and 29.8 g/10 min and decrease from control sample A0 (LDPE) as the other ingredients are added (TPS-s, LDPE-g-AM, and EPDM, respectively), the lowest value being that of sample A3, which contains the EPDM elastomer (and may be due to amorphous regions that can affect melt flow) [50].

This characteristic depends both on the flow indexes of individual components and on their morphology, and, when adding ingredients in the mixture, their structure changes; therefore, the flow of macromolecules towards each other is hindered.

### 3.2. FTIR Spectra Analysis

Figures 2 and 3 present the FTIR spectra of the analysed samples, and Table 5 indicates the main absorption bands noticed in their FTIR spectra and the corresponding functional groups.

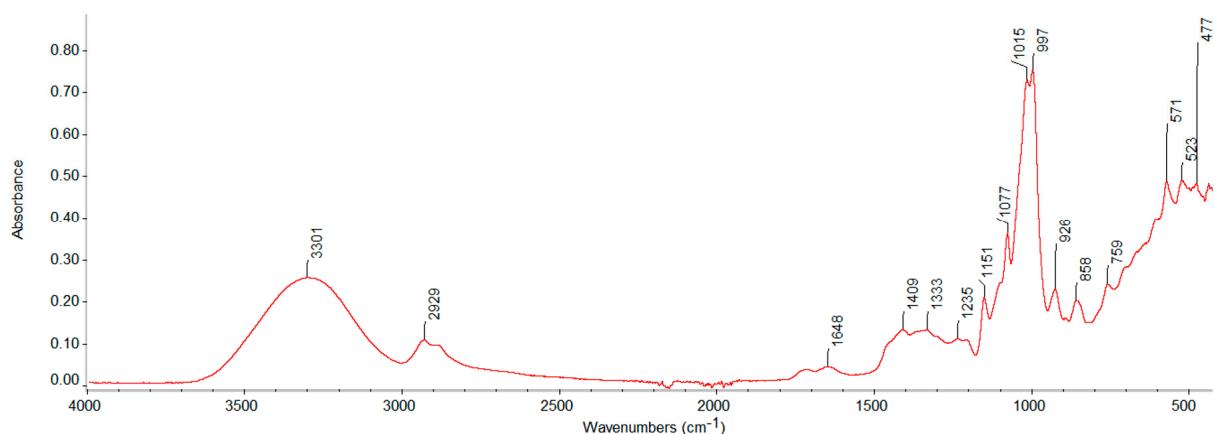
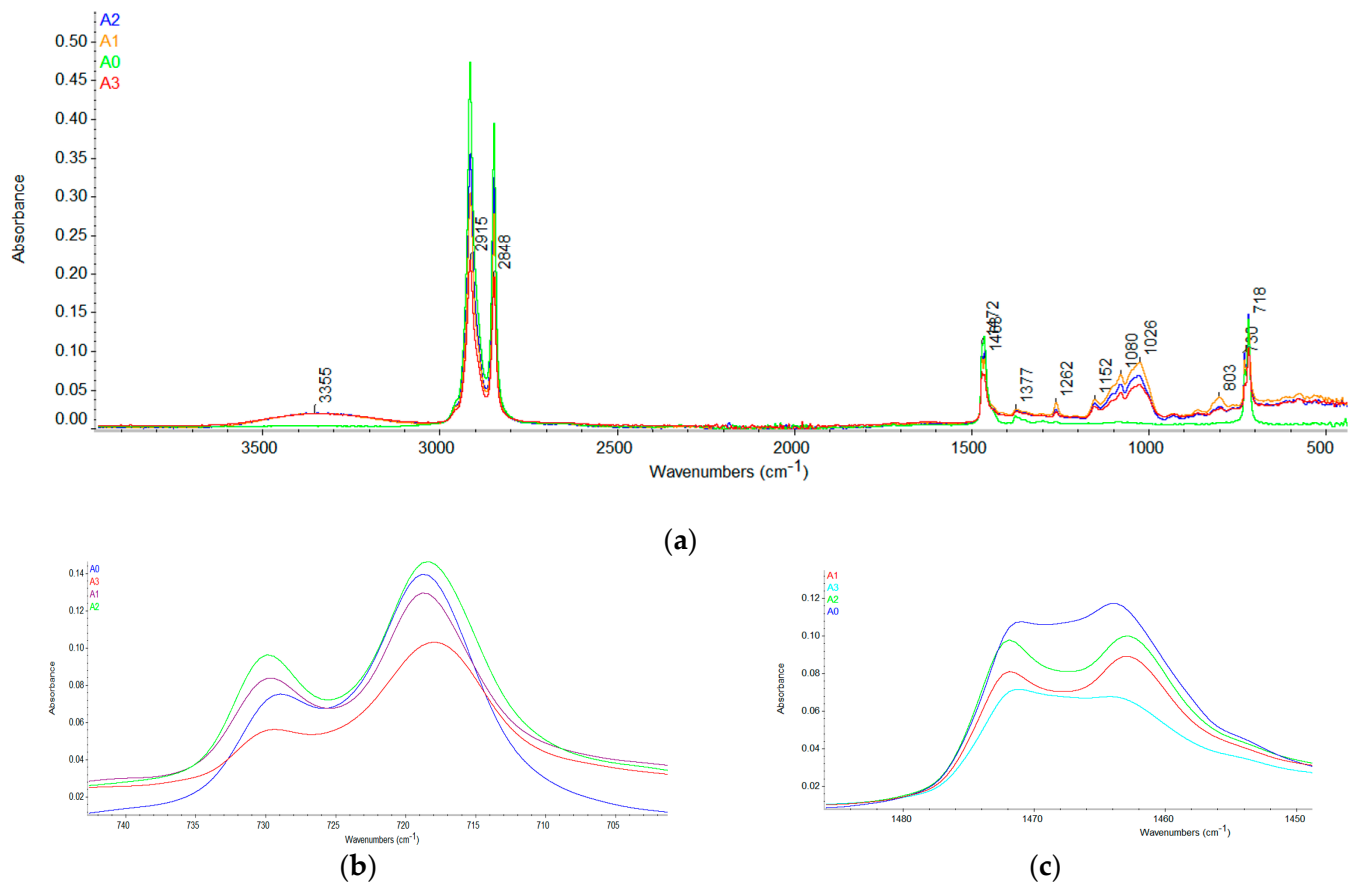


Figure 2. FTIR spectrum of thermoplastic starch TPS-s.



**Figure 3.** FTIR spectra of A0, A1, A2, and A3 samples (a), and details for 700–740  $\text{cm}^{-1}$  (b) and 1450–1480  $\text{cm}^{-1}$  (c).

**Table 5.** Correspondence between the bands in the FTIR spectra of the samples and the chemical groups.

Group Frequency ( $\text{cm}^{-1}$ )	Functional Group/Assignment
3299–3359	O–H, hydroxyl group, H-bonded OH stretch (from TPS-s)
2915–2929	methylene asym/sym stretch (from starch, LDPE, EPDM)
2848	methyl asym/sym stretch (from starch, LDPE, EPDM)
1471–1472	Crystalline bending methylene ( $\text{CH}_2$ )
1463–1464	Amorphous bending methylene ( $\text{CH}_2$ )
1333–1413	tertiary alcohol, OH bend, methylene C–H bend, trimethyl or tert-butyl (multiplet)
1262	Primary or secondary, OH in-plane bend
1010–1170	primary, secondary, tertiary alcohols, C–O stretch, C–O–C, cyclic ethers, large rings, C–O stretch, C–O–C, alkyl-substituted ether, C–O stretch
926–1024	Cyclohexane ring vibrations (from starch)
730	Crystalline rock methylene ( $\text{CH}_2$ )
718–719	Amorphous rock methylene ( $\text{CH}_2$ )

The FTIR spectrum of thermoplastic starch (Figure 2) shows a wide absorption band at 3301  $\text{cm}^{-1}$  corresponding to the stretching vibration of the O–H bond associated with hydrogen bonds or valence vibrations of polar O–H bonds existing in the TPS [51]. Ab-

sorption bands appearing at  $2929\text{ cm}^{-1}$  are due to the asymmetric vibration of C–H bonds from  $\text{CH}_2$  moieties. The TPS-s spectrum contains several absorption bands located in the fingerprint region, such as absorption bands attributed to stretching vibrations of the C–O bond in C–O–H ( $1151\text{ cm}^{-1}$  and  $1077\text{ cm}^{-1}$ ) and in C–O–C ( $997\text{ cm}^{-1}$ ,  $926\text{ cm}^{-1}$ , and  $858\text{ cm}^{-1}$ ) from starch [52].

As all the samples contain LDPE, absorption bands at  $2915\text{ cm}^{-1}$  and  $2848\text{ cm}^{-1}$  (Figure 3) can be noticed. These are attributed to asymmetric and symmetric stretching vibrations of the methylene group [53]. The intensity of these two bands is higher than in the TPS sample as they are related to the presence of LDPE in the sample. In control sample A0 (LDPE), there is an absorption band at  $719\text{ cm}^{-1}$  attributed to the in-plane deformation vibration (rotation) of the methylene group ( $-\text{CH}_2-$ ), this also being specified in other works [54–56]. In samples A1 and A2, respectively, containing thermoplastic starch (TPS-s), a division of this band in two can be observed (called crystal splitting), with the appearance of a second peak at  $730\text{ cm}^{-1}$ . This indicates that TPS-s influenced the degree of crystallization of the samples, and the existing starch in TPS-s behaved as a nucleating agent and led to short-range ordering of the samples. This phenomenon was more visible in sample A2, where there is also splitting of the peak at  $1464\text{ cm}^{-1}$  into an absorption band at  $1463\text{ cm}^{-1}$  and one at  $1472\text{ cm}^{-1}$ . Among these bands, those at  $1472\text{ cm}^{-1}$  and  $730\text{ cm}^{-1}$  are generated by the crystalline phase and those at  $1463$ – $1464\text{ cm}^{-1}$  and  $718$ – $719\text{ cm}^{-1}$  refer to the amorphous phase (see Figure 3b,c) [57–59].

The FTIR spectrum for the A3 sample contains additional features, specific to the EPDM elastomer. Such extra features are visible as the absorption bands due to the deformation vibration of the C–H bond at  $718\text{ cm}^{-1}$ , at  $1079\text{ cm}^{-1}$  (specific to the chemical group  $\text{CH}_3\text{-CH}_2\text{-CH}_2-$ ), at  $1377\text{ cm}^{-1}$  (corresponding to the chemical group  $-\text{CH}_3$ ), and the band at  $1152\text{ cm}^{-1}$  (corresponding to the group  $>\text{C}(\text{CH}_3)_2$ ) [60]. Despite spectra overlapping between EPDM and LDPE, a reduction in the splitting of the two peaks specific to the division of the crystal field through the chain interaction mentioned above can be observed for A3 (Figure 3). This indicates a reduction in the crystalline phase.

The spatial distribution of the polymer compounds in each sample was monitored by FTIR microscopy. Moreover, 2D maps were recorded for each sample, and they are depicted in Figure 4 for relevant wavenumbers ( $2931\text{ cm}^{-1}$  for C–H bond vibration;  $1480\text{ cm}^{-1}$   $\text{CH}_2$  bending;  $1170\text{ cm}^{-1}$  C–O stretch; and  $1005\text{ cm}^{-1}$  ring vibration), with red areas indicating the highest absorbance and blue areas corresponding to the lowest absorbance. The FTIR maps for the thermoplastic starch samples indicate that plasticization took place according to the working parameters (temperature, plasticization time, and homogenization). For samples A1 to A3, the recorded FTIR maps indicate good compounding (homogenization) of the thermoplastic starch with simple and functionalized polyethylene and EPDM, favouring good dispersion into the final mixture. As can be observed from Figure 4, the samples are quite homogenous, with only minor differences being present at the maximum level of tens of  $\mu\text{m}$ . The introduction of the compatibilizer, LDPE-g-MA, reduces the agglomeration tendency of constituent polymers and improves the dispersion into the LDPE matrix of the hydrophilic component (thermoplastic starch) and hydrophobic component, EPDM.

As expected, the thermoplastic starch has a lower thermal stability and starts losing bound water before  $100\text{ }^\circ\text{C}$ . The process is accompanied by an endothermic effect, with a minimum peak at  $89.1\text{ }^\circ\text{C}$  on the DSC curve. The recorded mass loss up to  $150\text{ }^\circ\text{C}$  is 2.99%. Additional water molecules are eliminated by the dehydration process of starch up to  $250\text{ }^\circ\text{C}$ . After this temperature the degradative oxidation processes start to break up the polymer backbone, and a strong exothermic effect can be observed on the DSC curve. The residual carbonaceous mass is burned away between  $350$  and  $500\text{ }^\circ\text{C}$ . Figure 6 presents the details of thermal analysis of thermoplastic starch up to  $250\text{ }^\circ\text{C}$ . An apparent glass transition can be observed around  $50\text{ }^\circ\text{C}$ , which is similar to some values reported in the literature [61,62].

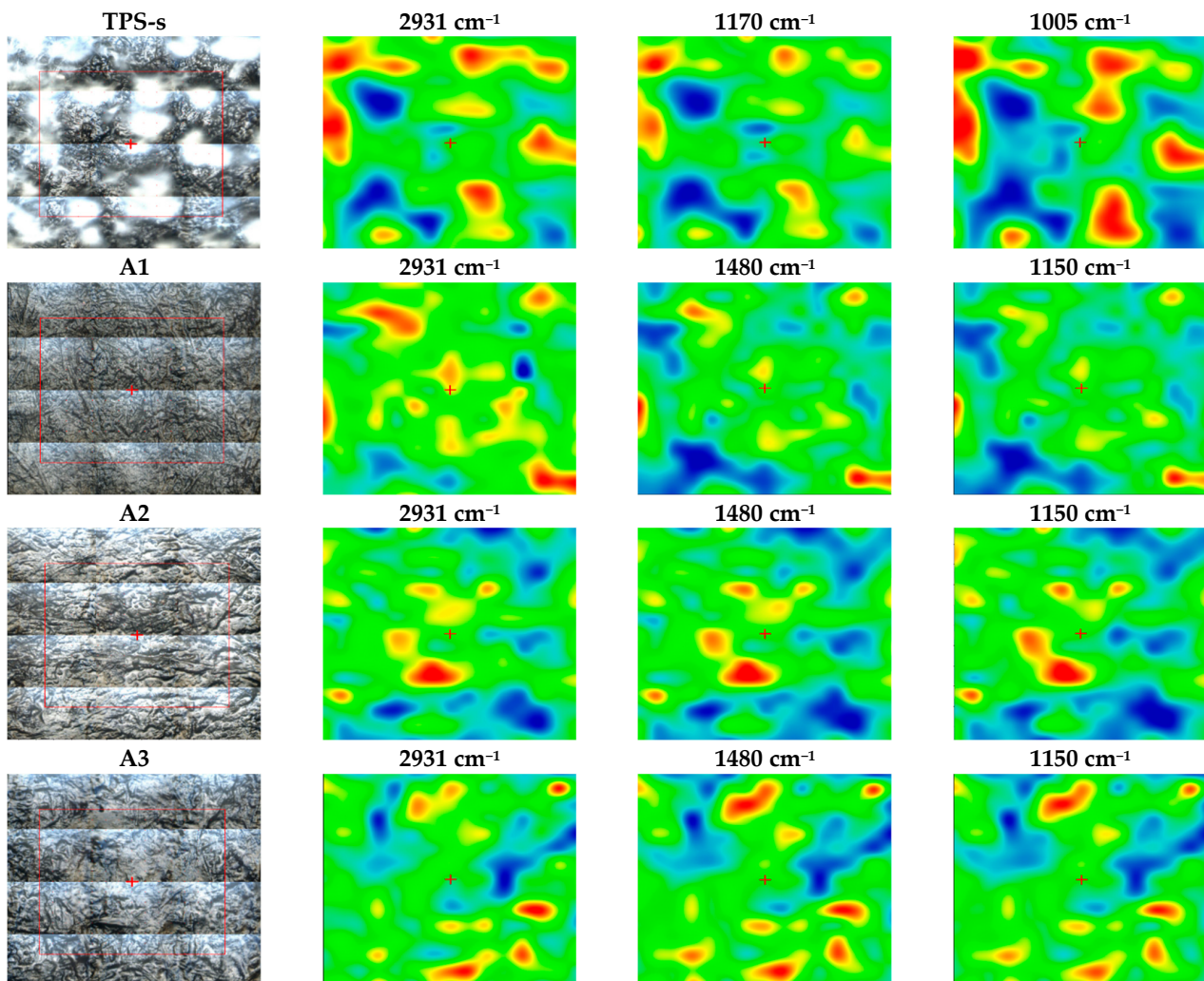


**Figure 4.** FTIR 2D maps for samples TPS-s, A1, A2, and A3.

### 3.3. Complex Thermal Analysis TG-DSC-FTIR

The thermal behaviour was investigated by thermal analysis in dynamic air atmosphere. The overall results are presented in Figure 5a–c.

The thermal analyses of the polyethylene samples (A0, A2, and A3) exhibit similar behaviour, with good stability up to 300 °C (Figure 5a), followed by rapid fragmentation of the backbone and oxidation of the resulting fragments, as observed from the strong exothermic effects on the DSC curves (Figure 5b). The burning of residual carbonaceous mass occurs from 450 to 550 °C but can extend to 650 °C for the sample containing EPDM.

As Figure 7 indicates, the A0 sample stability up to 300 °C is challenged by small oxidation processes that start just before this temperature, with CO<sub>2</sub> being observed in the evolved gases. The degradative processes begin after 335 °C, when not only CO<sub>2</sub> and H<sub>2</sub>O from oxidation reactions are observed but also important quantities of non-oxidized hydrocarbon fragments from backbone scission (Figure 7).

The details of thermal analysis up to 300 °C, presented in Figure 8, permit observation of minor differences among polyethylene for the A0, A2, and A3 samples. Thus, the addition of thermoplastic starch decreases the overall stability of the polymer mix as it will lose bound water that starch brings into the sample composition. The presence of a single endothermic effect due to the melting of the polymer blend indicates a homogenous sample, with only one crystal type, with little influence from the TPS-s addition, as reported previously by [35].

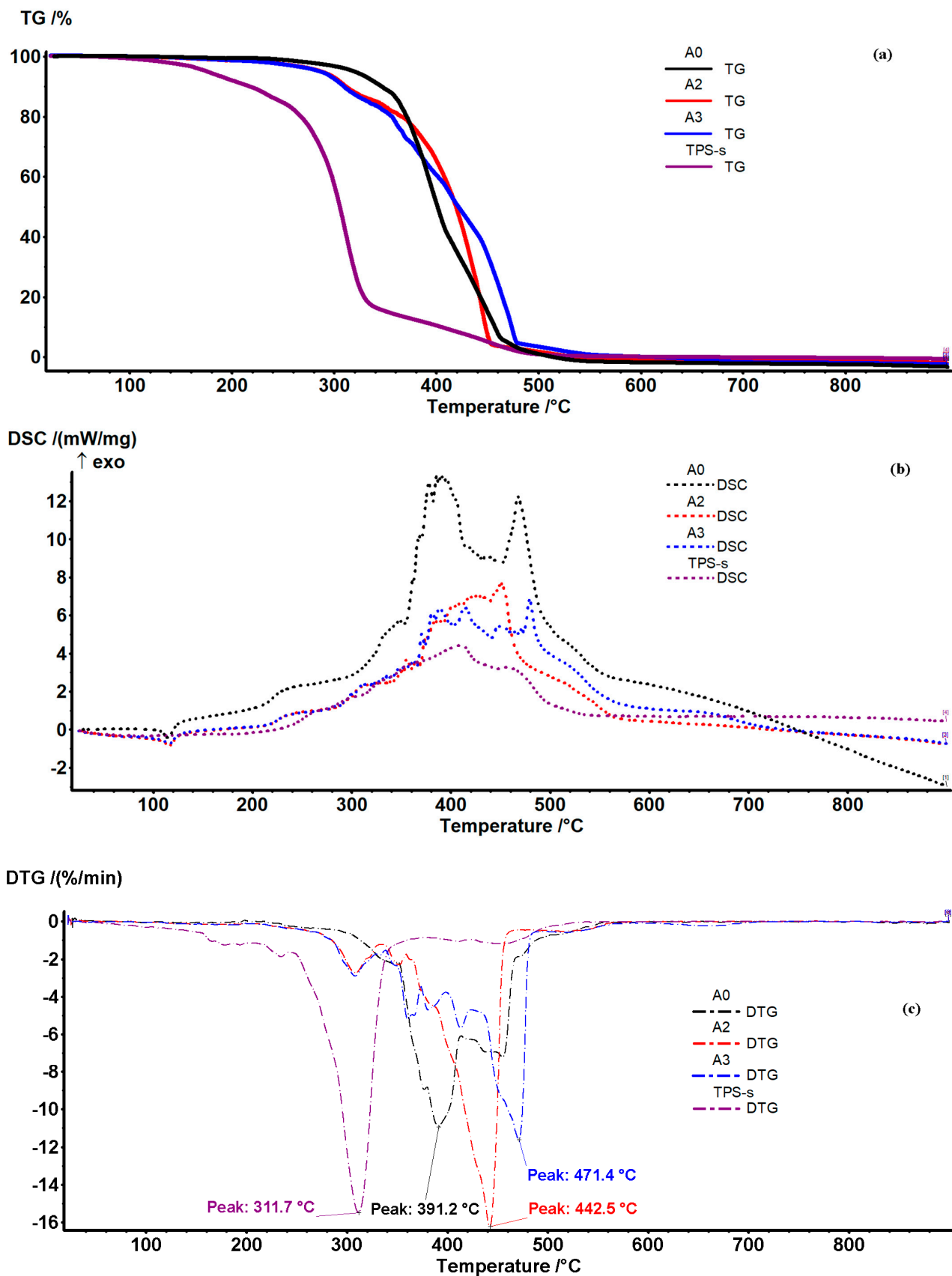


Figure 5. TG curves (a), DSC curves (b), and DTG curves (c) between 20 and 900 °C recorded for thermoplastic starch TPS-s and polyethylene mixtures A0, A2, and A3.

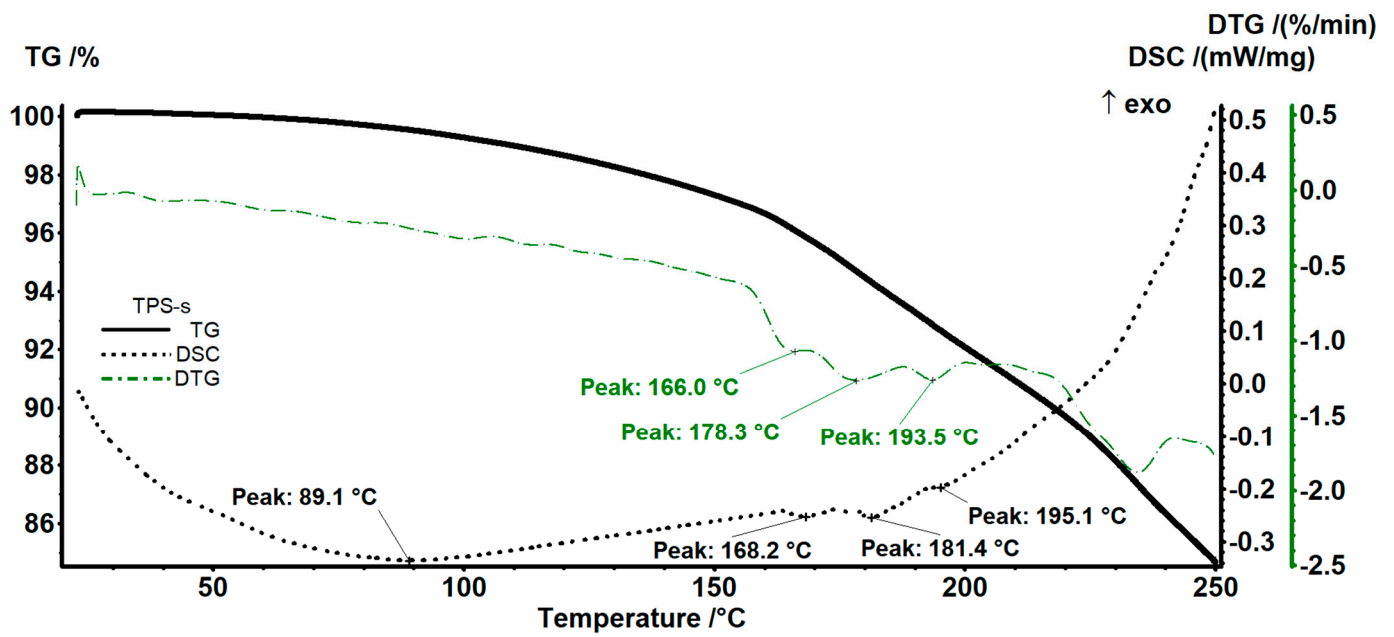


Figure 6. Details of TG, DTG, and DSC curves between 20 and 250 °C for the thermoplastic starch TPS-s sample.

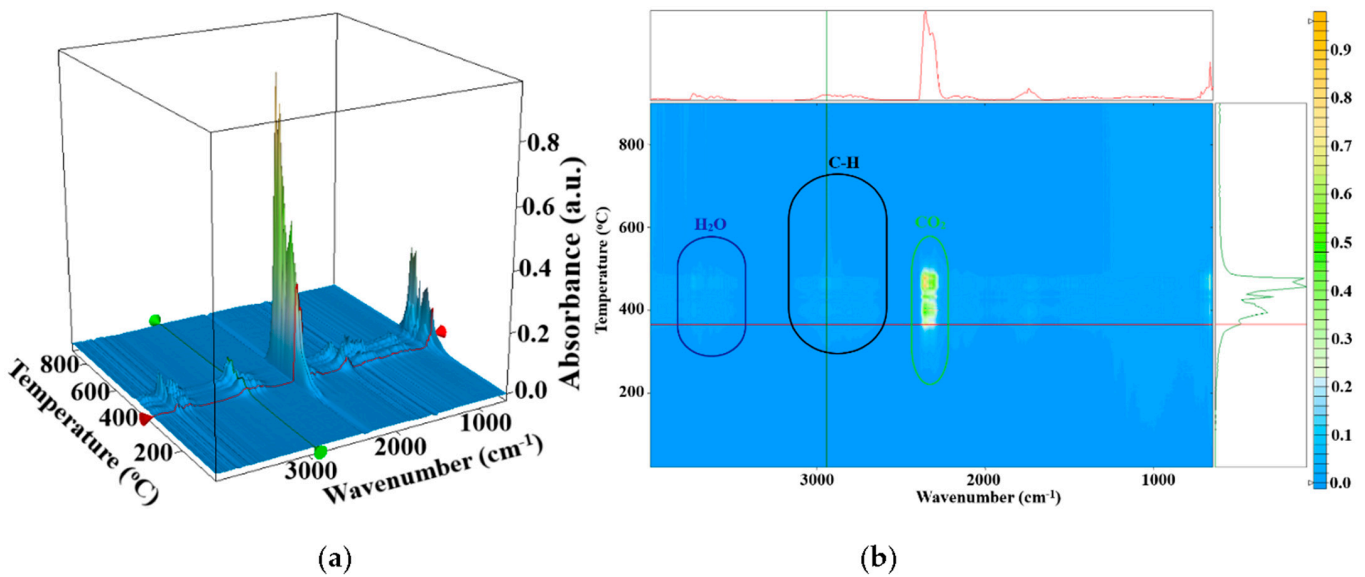


Figure 7. FTIR diagram of evolved gases from thermal analysis of A0 (a); 2D projection in temperature/wavenumber plan of the FTIR 3D diagram, with temperature intervals and specific substances marked—red line in the upper part is the FTIR spectrum from 365 °C; green line on right side is the trace of hydrocarbon fragments elimination (b).

The presence of thermoplastic starch also influences the composition of the evolved gases from thermal analysis (Figure 9). The apparition of hydrocarbon fragments starts earlier, from 300 °C, mainly due to degradation of starch as simple polyethylene exhibits higher thermal stability.

The DTG curves (Figure 5c) indicate the increasing thermal stability for the new materials when compared with TPS-s or A0. The DTG peak values corresponding to  $T_{d_{max}}$  increase from 311.7 °C for TPS-s and 391.2 °C for A0 to 442.5 and 471.4 °C for samples A2 and A3, respectively.

The principal data from the thermal analysis are presented in Table 6.

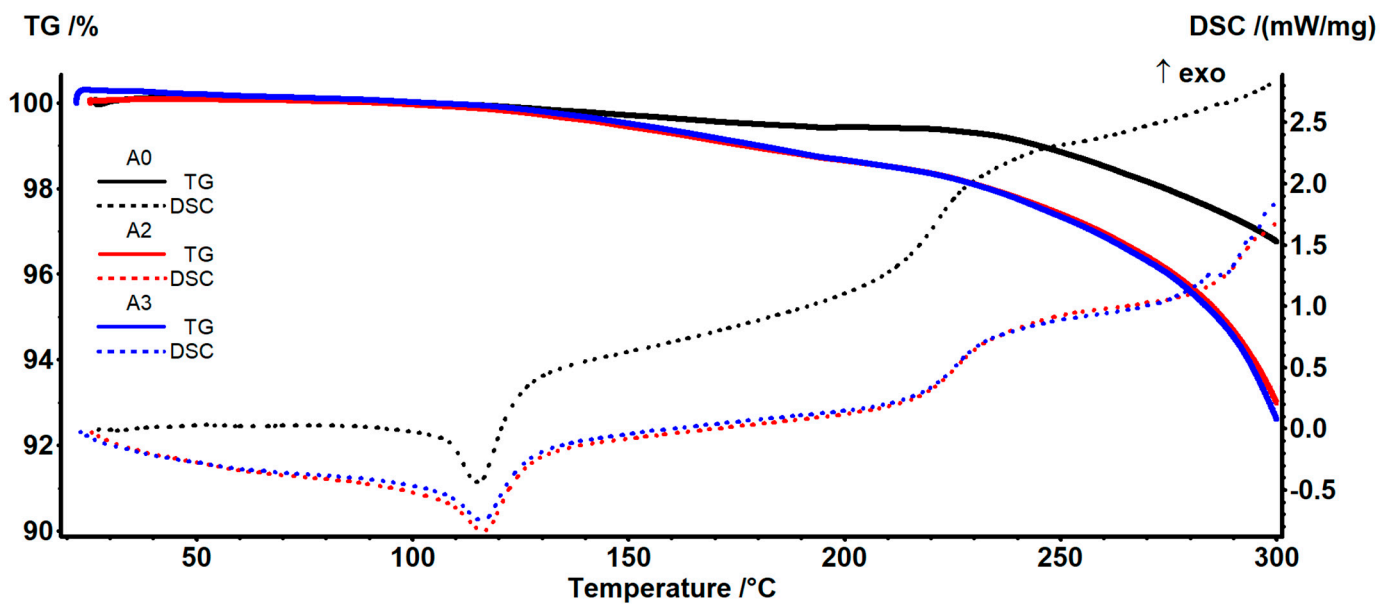


Figure 8. Details of TG-DSC curves between 20 and 300 °C for A0, A2, and A3 samples.

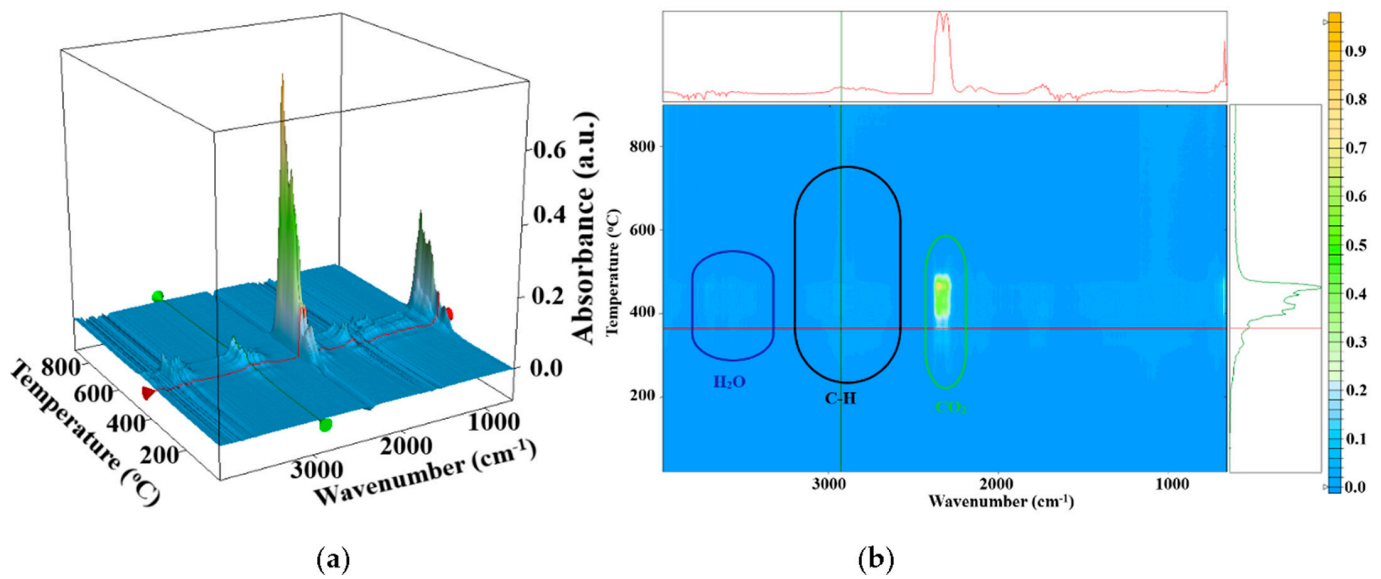


Figure 9. FTIR diagram of evolved gases from thermal analysis of A2 (a); 2D projection in temperature/wavenumber plan of the FTIR 3D diagram, with temperature intervals and specific substances marked—red line in the upper part is the FTIR spectrum from 364 °C; green line on the right side is the trace of hydrocarbon fragments elimination (b).

Table 6. Principal data from thermal analysis of thermoplastic starch and polyethylene samples.

Sample	T5%	T10%	Td <sub>max</sub>	Tm	ΔHm	Crystallinity Degree
TPS-s thermoplastic starch	176 °C	218 °C	311.7 °C	-	-	-
A0 (PE)	319 °C	346 °C	391.2 °C	107.8 °C	-78.20 J/g	26.68%
A2	287 °C	312 °C	442.5 °C	107.0 °C	-74.23 J/g	29.28%
A3	286 °C	310 °C	471.4 °C	106.7 °C	-67.56 J/g	29.98%

The crystallinity degree was calculated as the ratio between measured melting enthalpy ( $\Delta H_m$ ) and melting enthalpy of 100% crystalline polymer ( $\Delta H_m^0$ ) reported by Wunderlich (293 J/g) [63,64], additionally taking into account the PE content (%) in each mixture. The introduction of TPS or EPDM in the LDPE blends leads to an increase in crystallinity degree as the presence of these macromolecules can act as a nucleating agent, leading to short-range ordering of the LDPE chains around them. While TPS induced an increase of ~2.6% in the crystallinity degree, the addition of EPDM led to a further increase of ~0.7%.

### 3.4. Scanning Electron Microscopy—SEM

The mechanical properties of such polymer blends depend on the morphology and dispersion homogeneity. In these blends, the minor component (TPS-s) forms the dispersed phase in the matrix of the major component (LDPE). In order to assess the homogeneity of the polymer blending, cryo-fractured samples were exposed to hydrolytic degradation, which was performed in a HCl 6N solution at 60 °C for 48 h. The TPS-s phase is extracted via HCl to generate the contrast. The SEM micrographs obtained for each sample are presented in Figure 10.

The micrographs are presented at low magnification (100×) to gather the general aspect of the fracture, but also at higher magnification (up to 2000×) to notice the details of the surface.

As expected, the A0 sample containing only LDPE presents a typical fracture pattern, with stress marks along the fracture propagation direction but with no erosion due to HCl treatment as it is an inert polymer.

When hydrophilic polymers are blended with hydrophobic ones, various morphologies can be observed, like lamella/matrix, fibre/matrix, and droplet/matrix [33]. The A1 sample exhibits a smoother surface along the fracture, indicating a different fracture pattern when compared with the A0 sample, with lesser uneven formations due to micro-cracks propagation among TPS-s domains inside the LDPE matrix. The surface is marked by a well-dispersed hole pattern, formed after TPS-s hydrolysis. The hole location indicates zones where TPS-s was in the polymer blend; therefore, it can be concluded that the TPS-s phase exists as droplets dispersed inside the LDPE matrix. Their dispersion and lack of coalescence zones represent indications of homogeneity, as previously indicated by the FTIR microscopy analysis. The higher magnification micrograph for the A1 sample (1000×) indicates that, along micrometric pores, many smaller pores are present in the nanometre range.

The TPS-s particles' size provides information about the interactions between the blend components, in which larger particles indicate poor interactions and smaller particles show better interactions. The A2 SEM micrographs exhibit smaller density regarding both micrometre and nanometre pores, indicating that addition of LDPE-g-MA compatibilizer results in a highly homogenous polymer blend, most probably with mixing reaching the polymer chains level. This high level of homogeneity might explain the better mechanical properties of the A2 sample vs. the A1 sample.

In the case of the A3 sample, the EPDM addition is modifying the fracture aspect, lamellar and fibrous structures being observed due to reduction in the crystalline phase percentage. The presence of the elastomer generates specific micrometric structures as fracture progresses, which can be evidenced as partially detached lamella from the polymer matrix and also as depressions. The pores are corresponding to the zones where TPS-s was present in the polymer blend and indicate similar dispersion with the A2 sample, with a low number of both micrometre- and nanometre-size pores.

The SEM micrographs obtained on the surface of the A0–A3 samples are presented in Figure 11. The smooth surface presents some dents that can be attributed to imperfections of the compression moulding plates. Additionally, for the A1–A3 samples, a low number of holes can be observed. These were generated by the presence of some small TPS-s droplets on the surface. We can conclude that TPS-s is present in negligible quantities on the surface of the samples (as also observed from the cross-section micrographs in

Figure 10). This feature is important when assessing the stability and biodegradability of polymer blends [65]. The surface morphology of a sample indicates the probability and possibility of biodegradation by environmental factors as biodegradation is a surface phenomenon.

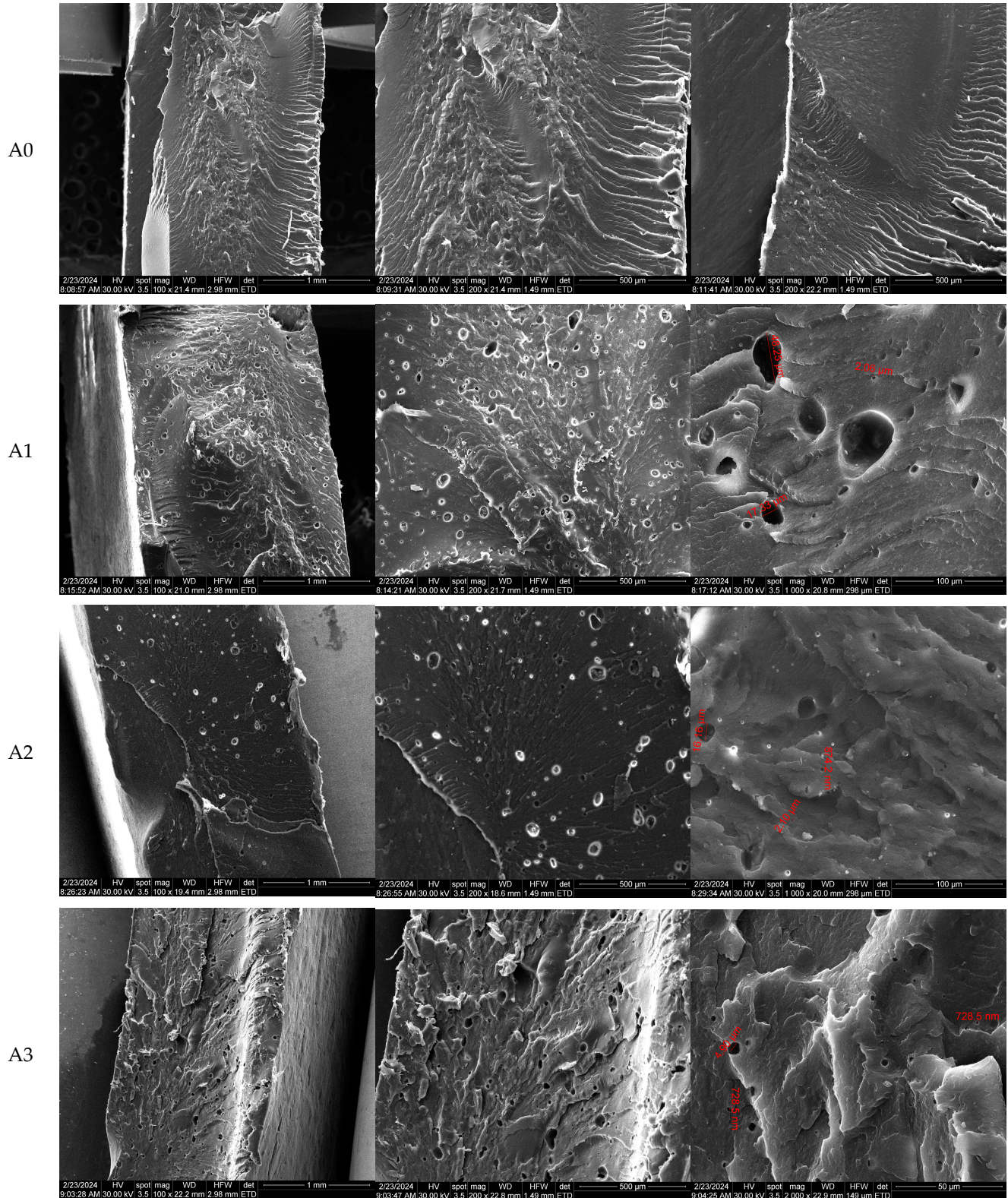
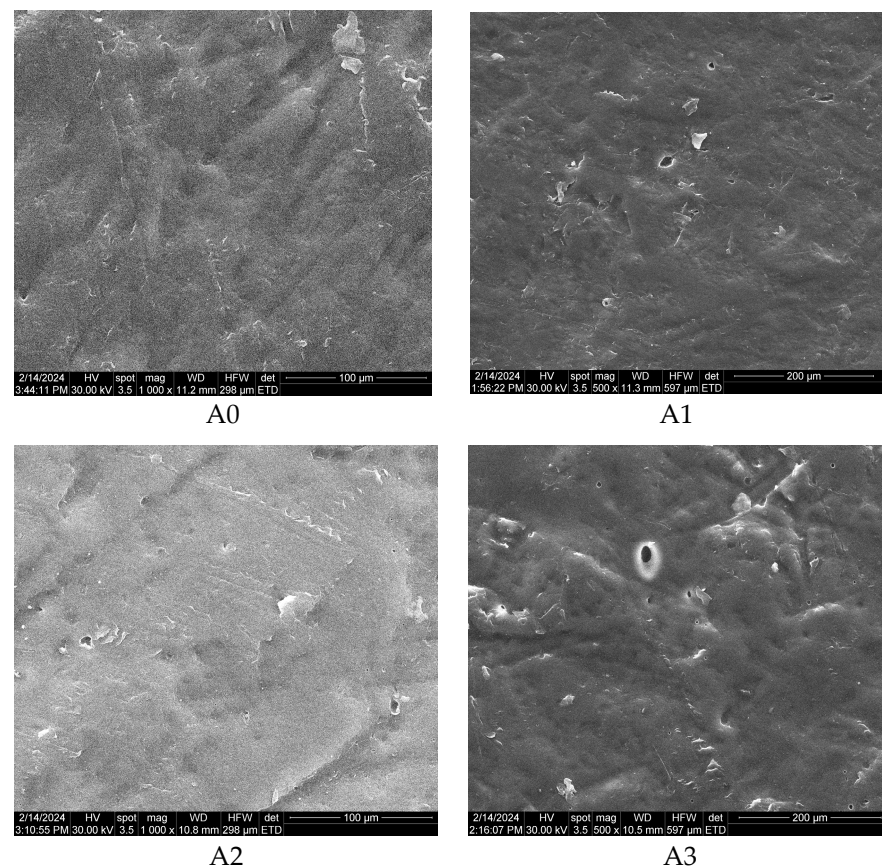


Figure 10. The SEM micrographs for the cryo-fractured cross-sections of A0, A1, A2, and A3 samples after 48 h treatment with HCl 6N at 60 °C.



**Figure 11.** The SEM micrographs for the A0, A1, A2, and A3 samples after 48 h treatment with HCl 6N at 60 °C.

Aside from TPS-s agglomeration size, phase continuity represents the critical factor affecting the biodegradability of this polymer blend. As we have demonstrated, TPS-s is found well-dispersed in droplets, from nanometre to micrometre size, the blends being highly homogenous after adding LDPE-g-MA compatibilizer. The lack of continuity in the TPS-s phase and the minimal presence of TPS-s on sample surfaces indicate that moisture penetration and microbial invasion do not have a clear pathway to occur. These are important factors that are blocking the biodegradability of the polymer blends and therefore are minimizing the possibility of microplastics formation during normal use. Therefore, we report here polymer blends based on LDPE with good dispersion of the TPS-s phase and different morphology on the surface and inside that were obtained by using low TPS-s proportions and compatibilizers. Previous literature reports highly inhomogeneous blends containing TPS of 20% and up [33,34], with a sponge-like structure that is highly prone to biodegradation. In other cases, when low TPS content is reported (5–20%) and LDPE-g-MA compatibilizer is used, poor homogeneity is assessed from the DSC peaks, while SEM study occurs without TPS etching, therefore being inconclusive [35]. This morphology, with homogenous dispersion of TPS-s into the LDPE matrix, can be assigned to both compatibilizing agents: citric acid from TPS-s and LDPE-g-AM.

#### 4. Conclusions

Mixtures based on LDPE and TPS-s were obtained and processed easily using specific laboratory equipment. The thermal analyses showed that TPS-s has good resistance for temperatures up to 250 °C, with only minor mass losses being observed up to this temperature due to the elimination of surface residual water molecules. The blends of LDPE and TPS-s have improved thermal stability when compared to TPS up to 300 °C. The crystallinity degree of the samples calculated from the thermal analysis indicates a

slight increase for adding other ingredients to LDPE (TPS-s, LDPE-g-AM, and EPDM, respectively). Crystallinity modification also led to a decrease in some physical–mechanical properties, such as hardness, tensile strength, and tear strength. At the same time, the FTIR analyses indicated that TPS-s influenced the degree of crystallization of the samples, and the starch present in TPS-s can act as a nucleating agent, leading to short-range ordering of the samples. The FTIR maps indicated that the technological process and the working parameters selected for obtaining TPS-s and LDPE-TPS-s samples led to homogeneous samples. At the same time, they showed that the introduction of LDPE-g-AM (compatibilizing agent) reduced the agglomeration tendency of the constituent polymers and improved the dispersion of TPS-s and EPDM in the LDPE matrix. Similarly, SEM microscopy indicated that the obtained polymer mixtures present good dispersion of the TPS-s phase, as well as a different morphology when LDPE-g-MA compatibilizer and EPDM are added. This may be due to the use of a low TPS-s ratio and the presence of LDPE-g-MA. The melt flow index at 200 °C and a pressing force of 2.16 kg show values of 15–30 g/10 min, indicating good processability of the samples through methods specific to plastics, such as extrusion and injection. The obtained polymer blends can be used as packaging (from films to boxes), foils for general use in construction or agriculture, shielding plates, or other plastic components for the automotive industry, etc.

**Author Contributions:** Conceptualization, M.D.S. and O.-C.O.; methodology, M.S. and M.N.; validation, M.D.S., O.-C.O. and M.G.; formal analysis, M.D.S., O.-C.O., L.M., A.F., R.-D.T., M.S. and M.N.; investigation, M.D.S., M.G., O.-C.O., L.M., A.F., R.-D.T., M.S. and M.N.; resources, M.D.S. and O.-C.O.; data curation, A.F.; writing—original draft preparation, M.D.S., M.G., M.S. and M.N.; writing—review and editing, O.-C.O., L.M., A.F., R.-D.T. and M.D.S.; supervision, M.D.S. and O.-C.O.; project administration, M.D.S.; funding acquisition, O.-C.O. All authors have read and agreed to the published version of the manuscript.

**Funding:** This work was supported by a grant of the Ministry of Research, Innovation and Digitization, CCCDI—UEFISCDI, project number PN-III-P2-2.1-PED-2021-3177, within PNCDI III; 712PED/2022 “Valorificarea superioara a polietilenei reciclate prin compoundare cu amidon modificat chimic si nanopulberi in vederea obtinerii de materiale cu proprietati antimicrobiene pentru imprimante 3D RepRap”.

**Data Availability Statement:** Dataset available on request from the authors.

**Conflicts of Interest:** The authors declare no conflict of interest.

## References

1. Motelica, L.; Fikai, D.; Oprea, O.C.; Fikai, A.; Andronescu, E. Smart food packaging designed by nanotechnological and drug delivery approaches. *Coatings* **2020**, *10*, 806. [[CrossRef](#)]
2. Motelica, L.; Fikai, D.; Fikai, A.; Oprea, O.C.; Kaya, D.A.; Andronescu, E. Biodegradable antimicrobial food packaging: Trends and perspectives. *Foods* **2020**, *9*, 1438. [[CrossRef](#)]
3. Zdanowicz, M. Influence of herbal extract on physicochemical properties of thermoplastic starch films. *Polymers* **2024**, *16*, 64. [[CrossRef](#)] [[PubMed](#)]
4. Rodriguez-Gonzalez, F.J.; Ramsay, B.A.; Favis, B.D. High performance ldpe/thermoplastic starch blends: A sustainable alternative to pure polyethylene. *Polymer* **2003**, *44*, 1517–1526. [[CrossRef](#)]
5. Park, D.I.; Dong, Y.Z.; Wang, S.Z.; Lee, S.J.; Choi, H.J. Rheological characteristics of starch-based biodegradable blends. *Polymers* **2023**, *15*, 1953. [[CrossRef](#)] [[PubMed](#)]
6. Amin, A.M.M.; Sauid, S.M.; Hamid, K.H.K.; Musa, M. Biodegradation behaviour of thermoplastic starch films derived from starch under controlled composting condition. *IOP Conf. Ser. Mater. Sci. Eng.* **2018**, *358*, 012050. [[CrossRef](#)]
7. Jeziorska, R.; Szadkowska, A.; Studzinski, M.; Chmielarek, M.; Spasowka, E. Morphology and selected properties of modified potato thermoplastic starch. *Polymers* **2023**, *15*, 1762. [[CrossRef](#)] [[PubMed](#)]
8. Tavares, L.; Sousa, L.R.; da Silva, S.M.; Lima, P.S.; Oliveira, J.M. Moisture sorption isotherms and thermodynamic properties of biodegradable polymers for application in food packaging industry. *Polymers* **2023**, *15*, 1634. [[CrossRef](#)] [[PubMed](#)]
9. Teran, J.L.L.; Maldonado, E.V.C.; Rangel, J.D.A.; Otazo, J.P.; Rico, M.I.B.; Xie, F. Development of antibacterial thermoplastic starch with natural oils and extracts: Structural, mechanical and thermal properties. *Polymers* **2024**, *16*, 180. [[CrossRef](#)]
10. Said, N.S.; Olawuyi, I.F.; Lee, W.Y. Tailoring pectin-pla bilayer film for optimal properties as a food pouch material. *Polymers* **2024**, *16*, 712. [[CrossRef](#)]

11. Bangar, S.P.; Whiteside, W.S.; Ashogbon, A.O.; Kumar, M. Recent advances in thermoplastic starches for food packaging: A review. *Food Packag. Shelf* **2021**, *30*, 100743. [[CrossRef](#)]
12. Lara, S.C.; Salcedo, F. Gelatinization and retrogradation phenomena in starch/montmorillonite nanocomposites plasticized with different glycerol/water ratios. *Carbohydr. Polym.* **2016**, *151*, 206–212. [[CrossRef](#)]
13. Tessanan, W.; Phinyocheep, P.; Amornsakchai, T. Sustainable materials with improved biodegradability and toughness from blends of poly(lactic acid), pineapple stem starch and modified natural rubber. *Polymers* **2024**, *16*, 232. [[CrossRef](#)] [[PubMed](#)]
14. Radfar, R.; Hosseini, H.; Farhoodi, M.; Srednicka-Tober, D.; Ghasemi, I.; Fathi, M.; Khaneghah, A.M. Factors affecting mechanical properties of low-density polyethylene (ldpe)/starch blends: A review. *Carpathian J. Food Sci. Technol.* **2020**, *12*, 6–26.
15. Grgic, D.K.; Miloloza, M.; Bulatovic, V.O.; Ukcic, S.; Slouf, M.; Gajdosova, V. Screening the efficacy of a microbial consortium of bacteria and fungi isolated from different environmental samples for the degradation of ldpe/tps films. *Separations* **2023**, *10*, 79. [[CrossRef](#)]
16. Nituica, M.; Oprea, O.; Stelescu, M.D.; Sonmez, M.; Georgescu, M.; Alexandrescu, L.; Motelica, L. Polymeric biocomposite based on thermoplastic polyurethane (tpu) and protein and elastomeric waste mixture. *Materials* **2023**, *16*, 5279. [[CrossRef](#)] [[PubMed](#)]
17. Li, G.; Favis, B.D. Morphology development and interfacial interactions in polycaprolactone/thermoplastic-starch blends. *Macromol. Chem. Phys.* **2010**, *211*, 321–333. [[CrossRef](#)]
18. Raquez, J.M.; Nabar, Y.; Narayan, R.; Dubois, P. In situ compatibilization of maleated thermoplastic starch/polyester melt-blends by reactive extrusion. *Polym. Eng. Sci.* **2008**, *48*, 1747–1754. [[CrossRef](#)]
19. Mohanty, S.; Nayak, S. Starch based biodegradable pbat nanocomposites: Effect of starch modification on mechanical, thermal, morphological and biodegradability behavior. *Int. J. Plast. Technol.* **2009**, *13*, 163–185. [[CrossRef](#)]
20. Ni, Z.B.; Shi, J.A.; Li, M.Y.; Lei, W.; Yu, W.W. Fdm 3d printing and soil-burial-degradation behaviors of residue of astragalus particles/thermoplastic starch/poly(lactic acid) biocomposites. *Polymers* **2023**, *15*, 2382. [[CrossRef](#)]
21. Huneault, M.A.; Li, H.B. Morphology and properties of compatibilized polylactide/thermoplastic starch blends. *Polymer* **2007**, *48*, 270–280. [[CrossRef](#)]
22. Rodriguez-Gonzalez, F.J.; Virgilio, N.; Ramsay, B.A.; Favis, B.D. Influence of melt drawing on the morphology of one- and two-step processed ldpe/thermoplastic starch blends. *Adv. Polym. Tech.* **2003**, *22*, 297–305. [[CrossRef](#)]
23. Taguet, A.; Huneault, M.A.; Favis, B.D. Interface/morphology relationships in polymer blends with thermoplastic starch. *Polymer* **2009**, *50*, 5733–5743. [[CrossRef](#)]
24. Dewi, R.; Sylvia, N.; Zulnazri, Riza, M. Melt flow index (mfi) analysis of sago based thermoplastic starch blend with polypropylene and polyethylene. *Mater. Today Proc.* **2023**, *87*, 396–400. [[CrossRef](#)]
25. Hong, S.I.; Wang, L.F.; Rhim, J.W. Preparation and characterization of nanoclays-incorporated polyethylene/thermoplastic starch composite films with antimicrobial activity. *Food Packag. Shelf* **2022**, *31*, 100784. [[CrossRef](#)]
26. Carvalho, B.O.; Gonçalves, L.P.C.; Mendonça, P.V.; Pereira, J.P.; Serra, A.C.; Coelho, J.F.J. Replacing harmful flame retardants with biodegradable starch-based materials in polyethylene formulations. *Polymers* **2023**, *15*, 4078. [[CrossRef](#)] [[PubMed](#)]
27. Fortelny, I.; Juza, J. The effects of copolymer compatibilizers on the phase structure evolution in polymer blends—A review. *Materials* **2021**, *14*, 7786. [[CrossRef](#)]
28. Parameswaranpillai, J.; Thomas, S.; Grohens, Y. *Polymer Blends: State of the Art, New Challenges, and Opportunities*; Wiley-VCH Verlag GmbH & Co. KGaA: Hoboken, NJ, USA, 2014.
29. Willett, J.L. Mechanical-properties of ldpe granular starch composites. *J. Appl. Polym. Sci.* **1994**, *54*, 1685–1695. [[CrossRef](#)]
30. Prinos, J.; Bikiaris, D.; Theologidis, S.; Panayiotou, C. Preparation and characterization of ldpe/starch blends containing ethylene/vinyl acetate copolymer as compatibilizer. *Polym. Eng. Sci.* **1998**, *38*, 954–964. [[CrossRef](#)]
31. Huneault, M.A.; Li, H.B. Preparation and properties of extruded thermoplastic starch/polymer blends. *J. Appl. Polym. Sci.* **2012**, *126*, E96–E108. [[CrossRef](#)]
32. Mazerolles, T.; Heuzey, M.C.; Soliman, M.; Martens, H.; Kleppinger, R.; Huneault, M.A. Development of co-continuous morphology in blends of thermoplastic starch and low-density polyethylene. *Carbohydr. Polym.* **2019**, *206*, 757–766. [[CrossRef](#)] [[PubMed](#)]
33. Li, G.; Sarazin, P.; Orts, W.J.; Imam, S.H.; Favis, B.D. Biodegradation of thermoplastic starch and its blends with poly(lactic acid) and polyethylene: Influence of morphology. *Macromol. Chem. Phys.* **2011**, *212*, 1147–1154. [[CrossRef](#)]
34. Tena-Salcido, C.S.; Rodriguez-Gonzalez, F.J.; Mendez-Hernandez, M.L.; Contreras-Esquivel, J.C. Effect of morphology on the biodegradation of thermoplastic starch in ldpe/tps blends. *Polym. Bull.* **2008**, *60*, 677–688. [[CrossRef](#)]
35. Sabetzadeh, M.; Bagheri, R.; Masoomi, M. Study on ternary low density polyethylene/linear low density polyethylene/thermoplastic starch blend films. *Carbohydr. Polym.* **2015**, *119*, 126–133. [[CrossRef](#)] [[PubMed](#)]
36. Martins, P.C.; Latorres, J.M.; Martins, V.G.; Machado, A.V. Effect of starch nanocrystals addition on the physicochemical, thermal, and optical properties of low-density polyethylene (ldpe) films. *Polym. Eng. Sci.* **2022**, *62*, 1786–1796. [[CrossRef](#)]
37. Nouri, M.; Mehrabzadeh, M. Studies on rheological behaviour of ldpe/epdm blends using a torque rheometer. *Iran. Polym. J.* **1996**, *5*, 237–241.
38. Zaman, H.; Beg, M.D.H. Study on binary low-density polyethylene (ldpe)/thermoplastic sago starch (tps) blend composites. *Prog. Appl. Sci. Technol.* **2021**, *11*, 53–65.
39. Rosa, D.S.; Guedes, C.G.F.; Pedroso, A.G. Gelatinized and nongelatinized corn starch/poly(epsilon-caprolactone) blends: Characterization by rheological, mechanical and morphological properties. *Polimeros* **2004**, *14*, 181–186. [[CrossRef](#)]

40. Majid, R.A.; Ismail, H.; Taib, R.M. Effects of pe-g-ma on tensile properties, morphology and water absorption of ldpe/thermoplastic sago starch blends. *Polym.-Plast. Technol.* **2009**, *48*, 919–924. [[CrossRef](#)]
41. Güney, O.; Bilici, I.; Dogan, D.; Metin, A.U. Mechanical and thermal properties of recycled polyethylene/surface treated hemp fiber bio-composites. *Polym. Compos.* **2023**, *44*, 4976–4992. [[CrossRef](#)]
42. ISO37; Rubber, Vulcanized or Thermoplastic—Determination of Tensile Stress–Strain Properties. ISO: Geneva, Switzerland, 2017. Available online: <https://standards.iteh.ai/catalog/standards/sist/6a945c64-8670-4205-98c7-6db5bd780201/iso-37-2017> (accessed on 5 March 2024).
43. ISO34-1; Rubber, Vulcanized or Thermoplastic—Determination of Tear Strength. Part 1 Trouser, Angle and Crescent Test Pieces. ISO: Geneva, Switzerland, 2015. Available online: <https://standards.iteh.ai/catalog/standards/sist/a2b8314d-13fd-46cb-aad6-44293c0246a2/iso-34-1-2015> (accessed on 5 March 2024).
44. ISO868; Plastics and Ebonite—Determination of Indentation Hardness by Means of a Durometer (Shore Hardness). ISO: Geneva, Switzerland, 2003. Available online: <https://standards.iteh.ai/catalog/standards/sist/b00a2780-f641-4857-8bb1-eb0d574b4af3/iso-868-2003> (accessed on 5 March 2024).
45. ISO4662; Rubber, Vulcanized or Thermoplastic—Determination of Rebound Resilience. ISO, 2017. Available online: <https://standards.iteh.ai/catalog/standards/sist/7b982f0b-3f32-4680-a24e-366e7de34bbd/iso-4662-2017> (accessed on 5 March 2024).
46. ISO1133; Plastics—Determination of the Melt Mass-Flow Rate (mfr) and Melt Volume-Flow Rate (mvr) of Thermoplastics. Part 1 Standard Method. ISO: Vernier, Geneva. Available online: <https://standards.iteh.ai/catalog/standards/sist/77dcf130-b606-4799-9315-a824a7f841ce/iso-1133-1-2022> (accessed on 5 March 2024).
47. Pham, N.T.H. Characterization of low-density polyethylene and ldpe-based/ethylene-vinyl acetate with medium content of vinyl acetate. *Polymers* **2021**, *13*, 2352. [[CrossRef](#)] [[PubMed](#)]
48. Liang, X.B.; Ito, M.; Nakajima, K. Reinforcement mechanism of carbon black-filled rubber nanocomposite as revealed by atomic force microscopy nanomechanics. *Polymers* **2021**, *13*, 3922. [[CrossRef](#)] [[PubMed](#)]
49. Robertson, C.G.; Hardman, N.J. Nature of carbon black reinforcement of rubber: Perspective on the original polymer nanocomposite. *Polymers* **2021**, *13*, 538. [[CrossRef](#)] [[PubMed](#)]
50. Stelescu, D.M.; Airinei, A.; Homocianu, M.; Fifere, N.; Timpu, D.; Aflori, M. Structural characteristics of some high density polyethylene/epdm blends. *Polym. Test.* **2013**, *32*, 187–196. [[CrossRef](#)]
51. Fonseca-García, A.; Osorio, B.H.; Aguirre-Loredo, R.Y.; Calambas, H.L.; Caicedo, C. Miscibility study of thermoplastic starch/poly(lactic acid) blends: Thermal and superficial properties. *Carbohydr. Polym.* **2022**, *293*, 119744. [[CrossRef](#)] [[PubMed](#)]
52. Paluch, M.; Ostrowska, J.; Tynski, P.; Sadurski, W.; Konkol, M. Structural and thermal properties of starch plasticized with glycerol/urea mixture. *J. Polym. Environ.* **2022**, *30*, 728–740. [[CrossRef](#)]
53. Motelica, L.; Vasile, B.-S.; Ficai, A.; Surdu, V.-A.; Ficai, D.; Oprea, O.C.; Andronescu, E.; Mustăţea, G.; Ungureanu, E.L.; Dobre, A.A. Antibacterial activity of zinc oxide nanoparticles loaded with essential oils. *Pharmaceutics* **2023**, *15*, 2470. [[CrossRef](#)] [[PubMed](#)]
54. Smith, B.C. The infrared spectra of polymers ii: Polyethylene. *Spectroscopy* **2021**, *36*, 24–29. [[CrossRef](#)]
55. Depan, D.; Chirdon, W.; Khattab, A. Morphological and chemical analysis of low-density polyethylene crystallized on carbon and clay nanofillers. *Polymers* **2021**, *13*, 1558. [[CrossRef](#)]
56. Agosti, E.; Zerbi, G.; Ward, I.M. Structure of the skin and core of ultradrawn polyethylene films by vibrational spectroscopy. *Polymer* **1992**, *33*, 4219–4229. [[CrossRef](#)]
57. Painter, P.C.; Havens, J.; Hart, W.W.; Koenig, J.L. Fourier-transform ir spectroscopic investigation of polyethylene single-crystals.1. Fine-structure of ch<sub>2</sub> rocking mode. *J. Polym. Sci. Pol. Phys.* **1977**, *15*, 1237–1249. [[CrossRef](#)]
58. Huang, J.B.; Hong, J.W.; Urban, M.W. Attenuated total reflectance fourier-transform infrared studies of crystalline amorphous content on polyethylene surfaces. *Polymer* **1992**, *33*, 5173–5178. [[CrossRef](#)]
59. Fontana, L.; Santoro, M.; Bini, R.; Vinh, D.Q.; Scandolo, S. High-pressure vibrational properties of polyethylene. *J. Chem. Phys.* **2010**, *133*, 204502. [[CrossRef](#)] [[PubMed](#)]
60. Roy, S.; De, P.P. Use of ldpe as matrix material in rubber sample preparation for ir analysis. *Polym. Test.* **1992**, *11*, 3–11. [[CrossRef](#)]
61. Leroy, L.; Stoclet, G.; Lefebvre, J.M.; Gaucher, V. Mechanical behavior of thermoplastic starch: Rationale for the temperature-relative humidity equivalence. *Polymers* **2022**, *14*, 2531. [[CrossRef](#)] [[PubMed](#)]
62. Liu, P.; Yu, L.; Wang, X.Y.; Li, D.; Chen, L.; Li, X.X. Glass transition temperature of starches with different amylose/amylopectin ratios. *J. Cereal. Sci.* **2010**, *51*, 388–391. [[CrossRef](#)]
63. Poh, L.; Wu, Q.; Chen, Y.D.; Narimissa, E. Characterization of industrial low-density polyethylene: A thermal, dynamic mechanical, and rheological investigation. *Rheol. Acta* **2022**, *61*, 701–720. [[CrossRef](#)]
64. Wunderlich, B. *Appendix—Atlas Table of Thermal Properties of Linear Macromolecules*; Academic Press: London, UK, 1990; pp. 417–431.
65. Suslova, T.N.; Salakhov, I.I.; Nikonorova, V.N.; Gilaeva, G.V.; Trifonova, O.M. Biodegradation features of composite materials based on high-density polyethylene and starch. *Microbiology* **2023**, *92*, 695–703. [[CrossRef](#)]

**Disclaimer/Publisher’s Note:** The statements, opinions and data contained in all publications are solely those of the individual author(s) and contributor(s) and not of MDPI and/or the editor(s). MDPI and/or the editor(s) disclaim responsibility for any injury to people or property resulting from any ideas, methods, instructions or products referred to in the content.